NANO LETTERS

2008
Vol. 8, No. 8
2204-2209

Correlated Piezoelectric and Electrical Properties in Individual ZnO Nanorods

David A. Scrymgeour* and Julia W. P. Hsu

Sandia National Laboratory, P.O. Box 5800, Albuquerque, New Mexico 87185-1415

Received March 10, 2008; Revised Manuscript Received May 2, 2008

ABSTRACT

Resistivity and piezoelectric response of individual ZnO nanorods were measured using scanning force microscopy. We found a variation in resistivity of 3 orders of magnitude, from 0.1 to 155 Ωcm and in piezoelectric coefficient ranging from 0.4 to 9.5 pm/V in ZnO nanorods grown from solution at the same time on the same substrate. However, there exists a clear correlation between these two properties: nanorods with low piezoelectric response display low resistivity. The relationship is explained by the reduction of the Madelung constant due to free electrons. The results highlight that slight differences in the local environment during synthesis can cause large variation in physical properties found among similar nanostructures. These variations cannot be revealed through ensemble measurements and may contribute to the confusion in the literature of individual nanostructure properties. We demonstrate that correlating multiple physical properties on individual nanostructures provides an insight into the origin of the varying physical properties.

The excitement surrounding nanomaterials has been fueled by the observation that the material properties depend on not only the composition but also on the size and shape. Many nanostructured materials have different properties that are often more desirable than those in the bulk. Next generation nanodevices such as nanostructured sensors,[1–3] field effect transistors,[4,5] and mechanical oscillators[6] will utilize these enhanced properties. However, the same mechanisms that modify nanomaterials properties—impurity incorporation, sensitivity to surfaces, unique atomic arrangements, confinement effects, etc. — also make them extremely sensitive to small differences. Ideally, this allows for the tuning of nanomaterial properties through synthesis conditions; however, in practice it can lead to widely differing and uncontrollable nanomaterial properties. This is evidenced in the variety and lack of reproducibility of mechanical,[7,8] thermal,[9–11] and electrical properties reported on measurements of individual nanostructures.[12,13] More importantly, these broad distributions make measurements of an ensemble of nanomaterials not reflect the average properties because the measurements could be dominated by a few outliers, e.g., the most conducting rods in an electrical measurement. In order to better understand the true distribution in nanomaterial properties, measurements need to be made on multiple individual structures. Furthermore, correlation of different physical properties on the same nanostructures can help shed light on the origin of variation. For example, we reported that the piezoelectric coefficients of discrete nanorods range from 0.67 to 8.75 pm/V among ZnO rods grown at the same time on the same sample. These variations are not related to the physical dimensions of the nanorods.[14] Here, we directly measure the piezoelectric response and resistivity on the same ZnO nanorods and find a clear correlation that high resistivity rods display higher piezoelectric coefficients.

Scanning force microscopy is a perfect tool to measure the properties of nanostructured materials because of the high lateral resolution afforded by the extremely sharp tip (radius of curvature typically <50 nm) and the wide range of properties that can be measured (electrical, magnetic, mechanical, etc.). In this study, we focus on two correlated property measurements: nanoscale piezoelectric and electrical properties. Piezoelectric force microscopy (PFM) measures small out-of-plane vibrations that are induced in a piezoelectric material by an oscillating voltage applied to a conducting AFM tip.[15,16] These oscillations are detected using a lock-in technique, and the amplitude and phase of the signals are directly related to the nanoscale piezoelectric response under the tip. The piezoelectric coefficient, d_{33}, is found from $\Delta l = d_{33}V$ where V is the applied voltage, and Δl is the out of plane height change determined from the PFM signal amplitude. Conductive AFM (CAFM) is used to probe the current—voltage relationship and to characterize conductivity variations at the nanoscale. Current is measured through a conductive AFM tip in contact with the biased sample using a high gain current amplifier.

We performed the correlated PFM and CAFM imaging on a Digital Instruments Dimension 3100 atomic force microscope. For the PFM imaging, the raw photodiode sensor response was accessed by a signal access module and directly fed into an external lock-in amplifier. The imaging signal

* To whom correspondence should be addressed. E-mail: dscrymg@sandia.gov.

10.1021/nl080704n CCC: $40.75
Published on Web 07/12/2008

was 5 V_{peak} voltage at ~16 kHz provided by an external function generator. Accurate piezoelectric amplitude measurements in units of pm/V were obtained using a background noise correction technique outlined in ref 17 in combination with the lock-in sensitivity, the applied voltage, and the photodiode sensitivity that was determined from the force distance curve taken with a given tip. We found the piezoelectric response of an individual rod by averaging a 3 × 3 pixel area near the middle of a nanorod to avoid edge enhancement of the signal.[18] The CAFM measurements were taken with the DI extended TUNA module, and the current was calibrated and zeroed on a 100 nA/V scale using both a 100 MΩ and 1 GΩ resistors. A bias of +50 mV was used to establish the locations of conducting rods, followed by current−voltage ($I-V$) curves on individual conducting rods. The two techniques (PFM and CAFM) could be switched easily without disturbing the alignment of the AFM tip that allowed for correlated images of the same rod.

The zinc oxide nanorods were grown on highly textured (111) silver films deposited on single crystal silicon wafers in an equimolar (20 mM) zinc nitrate ($Zn(NO_3)_2$) and hexamethylenetetramine (HMT) ($(CH_2)_6N_4$) aqueous solution held at 60 °C for 1−3 h. These conditions yield spatially separated rods that grow from the silver with the top surface being the polar [0001] face.[14] They vary in length from 400 to 600 nm with diameters between 150 and 500 nm due to different nucleation times.

Regardless of the tip coating used (Ti−Pt or conductive diamond), we observed that $I-V$ curves taken with CAFM on bare ZnO nanorods were always nonlinear. (See Supporting Information.) These nonlinear $I-V$ curves were the result of nonohmic tip-ZnO contact and do not allow the extraction of intrinsic ZnO nanorod electrical properties. Ohmic contacts were established by first annealing the ZnO nanorods in a flowing gas of 3% H_2 in 97% N_2 at 300 °C for 2 h. The rods were then embedded in photoresist to provide mechanical stability for subsequent contact mode imaging. After embedding, they were etched with a Ar−O_2 plasma to remove photoresist and expose the tops of the rods, which protrude 0 to 200 nm above the photoresist surface. Finally, the nanorods were capped with 50 nm of Au on 3 nm of Ti by electron beam evaporation. This procedure produced linear $I-V$ curves on >90% of the nanorods as measured with either conductive diamond or Ti−Pt coated tips. Both the linear shape of the IV curve and the much greater magnitude of current flow give us confidence that we are forming ohmic contacts with the rods. (See Supporting Information.) It is theorized that annealing in hydrogen creates a highly doped subsurface region that allows for ohmic contacts between the ZnO and the metal coating.[19–21] A diagram of the CAFM setup and sample is shown in Figure 1a. Conductive diamond coated tips (Veeco DD-RTESPA) were used for the correlation studies because the coating was more durable and can last for over 50 contact mode scans.

An example correlated PFM and CAFM image is shown in Figure 2. Figure 2a shows the piezoelectric response of 5 nanorods. Note that the response is uniform across the surface of each rod. Sweeping the voltage while holding the tip

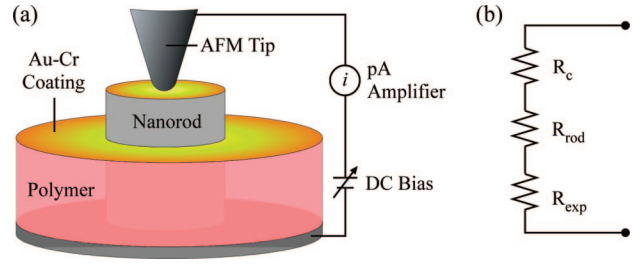

Figure 1. (a) Representation of experimental geometry for the CAFM measurements and (b) model of measurement circuit shown in panel a.

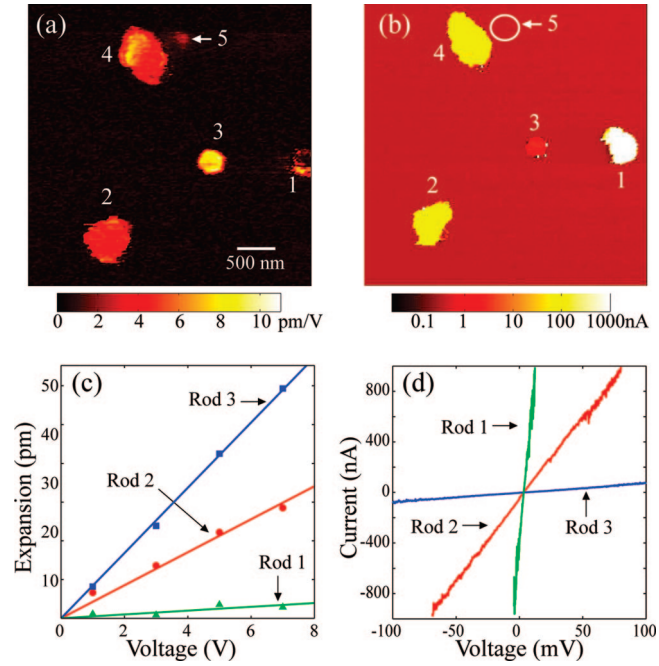

Figure 2. Correlated (a) PFM image and (b) CAFM image at a biasing voltage of +10 mV. Sweeps of the tip bias to determine piezoelectric response are shown in (c) and current−voltage sweeps of the same rods are shown in (d).

stationary above individual nanorods as in Figure 2c verified the linearity of the piezoelectric response and determined the piezoelectric coefficient of the rods in Figure 2a. Figure 2b shows the current flowing through each rod when the back plane was biased +10 mV. Current−voltage sweeps of individual rods in Figure 2b are shown in Figure 2d. The correlated PFM and CAFM results clearly demonstrate that current flow and piezoresponse are anticorrelated. Rod 1 shows the lowest PFM response at ~0.5 pm/V and the highest current flow corresponding to a resistance of 15 kΩ. The opposite is true for rod 3 with the highest PFM response at 8.4 pm/V, the lowest current flow, and the highest rod resistance of 1.3 MΩ. Rods 2 and 4 show intermediate piezoelectric responses of ~4.5 pm/V and resistances of ~80 kΩ. It should be pointed out that current flow is not necessary for PFM imaging; instead, PFM depends strictly on the electric field in the rod. Piezoelectric response can be imaged though a thin layer of photoresist that blocks current flow and renders rods invisible in the CAFM image as for example rod 5 in Figure 2.

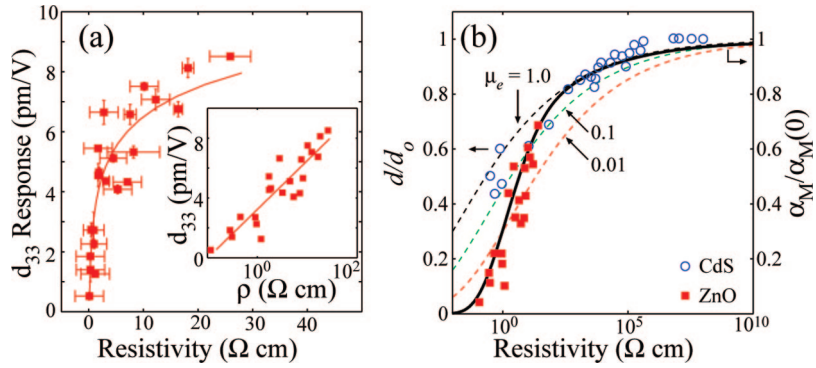

Figure 3. (a) Correlation of resistivity to piezoelectric response in ZnO nanorods. The solid line is a guide for the eye. Inset shows same data with resistivity in log scale. (b) Comparison of CdS data (open blue circles) taken from Ogawa[37] to the data in (a) normalized by the literature value of ZnO (12.4 pm/V) (red squares). Dashed lines are the normalized Madelung constant calculation for ZnO corresponding to the right axis for constant mobility of $\mu_e = 1.0$ (black), 0.1 (green), and 0.01 cm^2/Vs (red). The solid line is the calculation for resistivity dependent mobility (see text). CdS data in panel reprinted with permission from *Jpn. J. Appl. Phys.*

Over 70 individual nanorods with ohmic $I-V$ curves were measured. The range of values extended from 39 kΩ to 4.8 MΩ with the majority of nanorods having resistances between 60 kΩ and 500 kΩ. (The detailed resistance distribution is shown in the Supporting Information.) These values represent the resistance of the entire circuit that includes the resistance of the AFM coating, AFM tip-Au contact, metal-ZnO nanorod contact, ZnO nanorod resistance, and nanorod-substrate contact. The circuit is modeled as three resistors in series shown in Figure 1b: R_{rod} representing the resistance of the nanorod, R_c representing the resistance of the tip-Au surface contact and the tip resistance, and R_{exp} representing all fixed resistances in the experimental setup (the silver back contact, all associated wiring and circuits, etc.). The aggregate tip-Au contact and tip-coating resistance, R_c, was determined to be ~30 kΩ by placing the tip directly in contact with a gold coated silicon wafer and connecting the gold directly to the bias voltage. The experimental resistance, R_{exp}, is expected to be the same for all measurements, and just adds uniform and negligible resistance to all rods. It was estimated to be <50 Ω by measuring the resistance of the circuit bypassing the tip assembly and connecting the amplifier directly to the sample ground. The rod resistance, R_{rod}, was determined by subtracting the R_c and R_{exp} values from the total resistance for each rod. We found a spread of 3 orders of magnitude, from 9 kΩ to 4.8 MΩ that is unrelated to the physical dimensions of the rods. (See Supporting Information.)

The resistivity of each individual rod is calculated using R_{rod} with the rod height, determined from the topography image in combination with the known height of the photoresist surface, and the cross sectional area, determined from the area of the current flow in the current image (as in Figure 2b). The results show a resistivity range from 0.1 to 155 Ωcm, indicating that impurity incorporation during the solution growth can change greatly for rods grown at the same time on the same substrate. Typical resistivities of intrinsic zinc oxide single crystals range from 1−10 Ωcm,[22,23] but resistivities can range from 10^{-4} up to 10^8 Ωcm in lithium-compensated ZnO.[24,25] In most growth situations, ZnO is unintentionally n-type doped due to defects which have been attributed to either stoichiometric point defects[26–29] or hydrogen incorporation.[30–32] We estimate the carrier concentration in the nanorods, n_c, using $n_c = 1/\rho e \mu_e$, where ρ is the resistivity, e is the electronic charge, and μ_e is the electron mobility, reported to be 1 cm^2/Vs for solution grown ZnO nanorods measured in field effect transistor geometry.[33] This gives a carrier concentration in our nanorods between ~10^{16} and ~10^{19} cm^{-3}. These values are similar but higher than other estimations of carrier concentration of ZnO nanorods grown from both solution and vapor ($10^{15}-10^{18}$ cm^{-3}) reported by other groups.[33–36]

During PFM measurements, most materials are very insulating (i.e., ferroelectric single crystals) and no current can flow. However, the value of piezoelectric coefficients can be strongly affected when ohmic contacts are made to conducting piezoelectric materials. Because the resistance of the tip and the tip-metal contact can be a significant fraction of the resistance of the nanorod, a voltage that is lower than applied is dropped across the nanorod. Dividing the piezoelectric amplitude by the voltage drop across the rod (calculated using the applied voltage, R_{rod} and R_c) is used to obtain d_{33} of the nanorods. Piezoelectric response is plotted against the resistivity of the individual nanorods in Figure 3(a). It is clearly evident that there is a strong relationship between the piezoelectric response and the resistivity. The piezoelectric response has a linear dependence on the logarithm of the resistivity in this range with a correlation coefficient r of 0.90, indicating a good correlation.

Previous studies on the crystallographically similar piezoelectric semiconductor CdS also showed a strong dependence of the piezoelectric coefficient on the carrier concentration. The d_{33} coefficient of CdS decreased by 60% when the carrier concentration increased from 10^9 to 10^{18} cm^{-3} (blue open circles in Figure 3b).[37] We normalize the data in Figure 3a with the literature value of 12.4 pm/V for Li-compensated ZnO single crystal with resistivity >10^8 Ωcm (red solid squares in Figure 3b)[25] to compare to the CdS data. We find that the normalized ZnO d_{33} values show similar dependence on resistivity as CdS with comparable but lower piezoelectric response than CdS of equivalent resistivity. As the resistivity of the ZnO nanorods increases, we would expect to see the

d_{33} value approach the "intrinsic" value measured on very resistive material, similar to the trend observed in CdS.

It is important to note that the observed decrement in d_{33} response is not due to free carriers in the material screening the applied electric field. This certainly must be considered in systems where there is no current flow. When current flow is impeded, free charges can realign inside the material in response to the applied field as observed in the PFM of conducting ferroelectrics.[38,39] In the case of an ohmically contacted semiconductor as in this study, carriers can flow freely into and out of the rod and no screening can take place for times greater than the RC time constant for the rods ($\sim 10^{-10}$ seconds for even the most resistive rods in this study). During our PFM measurements, the ohmically contacted rods under bias have a uniform potential drop with a constant current density. Hence, charges cannot rearrange to create a space charge distribution so that electrostatic screening by conduction electrons cannot account for the observed reduction in the piezoelectric coefficient.

Several groups have attributed the observed reduction in piezoelectric coefficients in CdS to structural defects like stacking faults or dislocations in the crystal.[40–42] If small inclusions of inversion domains were to exist in a nanorod, the piezoelectric response would be decreased. However, we do not believe inversion domain inclusions, in which the *c*-axis points in the opposite direction from the surrounding matrix, occur in these samples because of the high energy associated with Zn−Zn or O−O wrong bonds at the {0001} domain boundaries. Typically, stacking faults are found to extend to the surface of the grain or crystal. If the inversion domains extend to the nanorod surface, resulting from stacking faults over a part of the *c*-plane,[43] we would be able to detect the change in crystal orientation in the PFM experiments. Since we have observed only [0001] oriented ZnO nanorods and did not observe any rods with mixed orientations,[14] there is no evidence for inversion domains. Additionally, photoconductive measurements on CdS crystals with a resistivity of $\sim 10^9$ Ωcm showed a decrease in the piezoelectric coefficients with optical injection of carriers. Because these optically injected carriers modified the piezoelectric coefficient, it was argued that the decrement in piezoelectric coefficient cannot be fully explained by defects alone and that the free electrons must play a large role.[44] No change was observed in the piezoelectric coefficient with illumination of our ZnO nanorods, most likely because the amount of photogenerated carriers is small compared to the overall carrier concentration in these low resistivity rods.

An alternative theory was posited that the reduction in the observed piezoelectric coefficient in CdS is due to a decrease of the Madelung constant caused by Thomas−Fermi screening of conduction electrons.[37] In an ionic crystal, the Madelung constant is a measure of the ionic attraction of the crystal structure and, hence, is related to the bond strength of the crystal. Since the piezoelectric effect is the stretching and compression of bonds in response to strain or voltage, the Madelung constant is important to the piezoelectric response. The Madelung constant is applicable in the quasi-static case and should have no frequency dependence for frequencies below that of the RC time constant of the rod, approximately 10 GHz. We find that the piezoelectric responses of our nanorods are constant over the frequency range of 5−50 kHz (see Supporting Information). Along the polar axis of the ZnO crystal, the Madelung constant can be modeled with a linear chain model of an ionic crystal as

$$\alpha_M = e^{-k_s R_o} - \frac{1}{2}e^{-2k_s R_o} + \frac{1}{3}e^{-3k_s R_o} - \cdots = 2\ln[1 + e^{-k_s R_o}] \quad (1)$$

where R_o is the distance between ions and k_s is the Thomas-Fermi screening constant given by

$$ks = \sqrt{2}\left(\frac{3}{\pi}\right)^{1/6} \frac{n_c^{1/6}}{a_H^{1/2}} \quad (2)$$

where n_c is the density of conduction electrons, and a_H is the Bohr radius.[37] Using $R_0 = 2.53$ Å for the average distance between Zn and O along the polar axis,[45] the Madelung constant as a function of carrier concentration is calculated. These values are normalized by the Madelung constant with no free carriers, $\alpha_M(0)$, and are overlaid on the d_{33} in Figure 3b using different constant electron mobilities, μ_e. While this simple model with constant μ_e captures the essence that decreasing resistivity leads to a decreasing Madelung constant and a lower piezoelectric coefficient, it does not match the experimental data for the resistivity dependence of d_{33} very well for μ_e between 0.01 and 1 cm^2/Vs.

One of the assumptions underlying the model above is that mobility is constant over several orders of magnitude change in resistivity. This is most likely incorrect. Impurities or defects that contribute to the increasing carrier concentrations also act as scattering centers that can significantly decrease the electron mobility, as documented in doped silicon and other semicondutors.[46,47] For ZnO single crystals, room temperature mobility is relatively high ($\sim$180 cm^2/Vs) and scattering is dominated by both acoustical and optical phonon scattering.[48] Mobility in thin films and nanostructures, however, is much lower, limited by defect, impurity, and surface scattering.[49,50] Transmission electron microscopy images (see Supporting Information) reveal many structural defects in these nanorods, which could contribute to mobility reduction. While the exact dependence of mobility on resistivity in ZnO nanorods has not been measured, let us consider a phenomenological model that describes the decreasing electron mobility μ due to decreasing resistivity, ρ, as

$$\mu = \mu_o \frac{\rho}{\rho_o + \rho} \quad (3)$$

where μ_o is the nanorod mobility at high resistivity $\rho \gg \rho_o$. This captures the constant mobility for high resistivity (low defect) materials and the reduction of mobility for highly defective materials. Using this model, a very good agreement with the ZnO nanorod data (solid black line in Figure 3b) is found using a μ_o of 1 cm^2/Vs, the mobility measured in ZnO nanostructures,[33] at ρ_o equal to 10^2 Ωcm. While the actual form of mobility dependence on resistivity is probably more complicated, this model can reproduce the experimental results with physically reasonable μ_o and ρ_o for ZnO nanorods and illustrates the important role of a resistivity dependent mobility for low resistivity materials.

This work highlights many of the difficulties associated with determining nanomaterial properties. Individual nanowire properties can vary greatly, making extrapolation from a small number of measurements on individual nanostructures to an entire population prone to error. On the other hand, measurements of many nanostructures simultaneously, for example the lumped resistance of an array of nanorods, do not accurately reflect the distribution of a population's properties because they can be dominated by a few individual outliers. The approach used here, measuring multiple properties on many individual nanostructures, can give a more complete understanding of properties than either of the other approaches.

In this letter, we report a correlated relationship between the piezoelectric response and the resistivity of individual ZnO nanorods by scanning force microscopy. As grown ZnO nanorods show an unintentional 3 orders of magnitude difference in resistivity, from 0.1 to 155 Ωcm with an estimated carrier concentration of $\sim 10^{16} - 10^{19}$ cm^{-3} and a piezoelectric coefficient varying from 0.4 to 9.5 pm/V. These differences are most likely due to a combination of both structural and compositional defects or impurity incorporation in the material, which highlights the lack of control at the nanoscale during synthesis. Through correlating piezoelectric and current measurements, we can directly attribute the variation in piezoelectric response to the variation in resistivity. More resistive nanorods exhibit a higher piezoelectric response. The free electron screening of the Madelung constant which reduces the ionic bond strength of the crystal models the decrease in the piezoelectric coefficient with lower resistivity. We show that, in addition to the carrier density, reduction in mobility due defect/impurity scattering has a significant effect in highly conducting materials.

Acknowledgment. The authors thank B. Swartzentruber for helpful discussions, J. Sigman for assistance with the hydrogen annealing, and P. Kotula for the TEM imaging. This research was supported in part by an appointment to the Sandia National Laboratories Truman Fellowship in National Security Science and Engineering, sponsored by Sandia Corporation (a wholly owned subsidiary of Lockheed Martin Corporation) as Operator of Sandia National Laboratories under its U.S. Department of Energy Contract No. DE-AC04-94AL85000.

Supporting Information Available: Linear versus nonlinear $I-V$s measured on ZnO nanorods. Histogram of resistances measured on Cr−Au coated nanorods. Frequency dependence of ZnO nanorods piezoelectric response. Dependence of resistivity on physical dimensions of nanorods. Cross-sectional TEM image of ZnO nanorod. Additional discussion of Madelung constant calculations.This material is available free of charge via the Internet at http://pubs.acs.org.

References

(1) Kong, J.; Franklin, N. R.; Zhou, C.; Chapline, M. G.; Peng, S.; Cho, K.; Dai, H. *Science* **2000**, *287* (5453), 622–625.
(2) Zhang, D.; Liu, Z.; Li, C.; Tang, T.; Liu, X.; Han, S.; Lei, B.; Zhou, C. *Nano Lett.* **2004**, *4* (10), 1919–1924.
(3) Xia, Y.; Yang, P.; Sun, Y.; Wu, Y.; Mayers, B.; Gates, B.; Yin, Y.; Kim, F.; Yan, H. *Adv. Mater.* **2003**, *15* (5), 353–389.
(4) McEuen, P. L.; Fuhrer, M. S.; Park, H. K. *IEEE Trans. Nanotechnol.* **2002**, *1* (1), 78–85.
(5) Huang, Y.; Duan, X. F.; Cui, Y.; Lieber, C. M. *Nano Lett.* **2002**, *2* (2), 101–104.
(6) Peng, H. B.; Chang, C. W.; Aloni, S.; Yuzvinsky, T. D.; Zettl, A. *Phys. Rev. Lett.* **2006**, *97* (8), 087203−4.
(7) Song, J. H.; Wang, X. D.; Riedo, E.; Wang, Z. L. *Nano Lett.* **2005**, *5* (10), 1954.
(8) Stan, G.; Ciobanu, C. V.; Parthangal, P. M.; Cook, R. F. *Nano Lett.* **2007**, *7* (12), 3691–3697.
(9) Hone, J.; Llaguno, M. C.; Nemes, N. M.; Johnson, A. T.; Fischer, J. E.; Walters, D. A.; Casavant, M. J.; Schmidt, J.; Smalley, R. E. *Appl. Phys. Lett.* **2000**, *77* (5), 666–668.
(10) Kim, P.; Shi, L.; Majumdar, A.; McEuen, P. L. *Phys. Rev. Lett.* **2001**, *87* (21), 215502.
(11) Yi, W.; Lu, L.; Dian-lin, Z.; Pan, Z. W.; Xie, S. S. *Phys. Rev. B* **1999**, *59* (14), R9015.
(12) Dattoli, E. N.; Wan, Q.; Guo, W.; Chen, Y. B.; Pan, X. Q.; Lu, W. *Nano Lett.* **2007**, *7* (8), 2463–2469.
(13) Rosenblatt, S.; Yaish, Y.; Park, J.; Gore, J.; Sazonova, V.; McEuen, P. L. *Nano Lett.* **2002**, *2* (8), 869–72.
(14) Scrymgeour, D. A.; Sounart, T. L.; Simmons, N. C.; Hsu, J. W. P. *J. Appl. Phys.* **2007**, *101* (1), 14316–1.
(15) Alexe, M.; Gruverman, A. *Nanoscale Characterisation of Ferroelectric Materials*; Springer: New York, 2004.
(16) Kalinin, S. V.; Rodriguez, B. J.; Jesse, S.; Karapetian, E.; Mirman, B.; Eliseev, E. A.; Morozovska, A. N. *Ann. Rev. Mater. Res.* **2007**, *37* (1), 189–238.
(17) Jungk, T.; Hoffmann, A.; Soergel, E. *Appl. Phys. Lett.* **2006**, *89*, 163507.
(18) Peter, F.; Rudiger, A.; Waser, R. *Rev. Sci. Instrum.* **2006**, *77*, 3.
(19) Strzhemechny, Y. M.; Mosbacker, H. L.; Goss, S. H.; Look, D. C.; Reynolds, D. C.; Litton, C. W.; Garces, N. Y.; Giles, N. C.; Halliburton, L. E.; Niki, S.; Brillson, L. J. *J. Electron. Mater.* **2005**, *34* (4), 399–403.
(20) Brillson, L. J.; Mosbacker, H. L.; Hetzer, M. J.; Strzhemechny, Y.; Jessen, G. H.; Look, D. C.; Cantwell, G.; Zhang, J.; Song, J. J. *Appl. Phys. Lett.* **2007**, *90* (10), 102116–1.
(21) Mosbacker, H. L.; Strzhemechny, Y. M.; White, B. D.; Smith, P. E.; Look, D. C.; Reynolds, D. C.; Litton, C. W.; Brillson, L. J. *Appl. Phys. Lett.* **2005**, *87* (1), 12102–1.
(22) Look, D. C.; Reynolds, D. C.; Sizelove, J. R.; Jones, R. L.; Litton, C. W.; Cantwell, G.; Harsch, W. C. *Solid State Commun.* **1998**, *105* (6), 399–401.
(23) Ziegler, E.; Heinrich, A.; Oppermann, H.; Stover, G. *Phys. Status Solidi A* **1981**, *66* (2), 635–648.
(24) Ellmer, K. *J. Phys. D: Appl. Phys.* **2001**, *34* (21), 3097–108.
(25) Crisler, D. F.; Cupal, J. J.; Moore, A. R. *Proc. IEEE* **1968**, *56* (2), 225.
(26) Jin, B. J.; Bae, S. H.; Lee, S. Y.; Im, S. *Mater. Sci. Eng., B* **2000**, *71* (1−3), 301–305.
(27) Look, D. C.; Farlow, G. C.; Reunchan, P.; Limpijumnong, S.; Zhang, S. B.; Nordlund, K. *Phys. Rev. Lett.* **2005**, *95* (22), 225502–4.
(28) Sabioni, A. C. S. *Solid-State Ionics, Diffus. React.* **2004**, *170* (1/2), 145–8.
(29) Tomlins, G. W.; Routbort, J. L.; Mason, T. O. *J. Appl. Phys.* **2000**, *87* (1), 117–23.
(30) Cox, S. F J.; Davis, E. A.; King, P. J. C.; Gil, J. M.; Alberto, H. V.; Vil, o R. C.; Duarte, J. P.; Campos, N. A. d.; Lichti, R. L. *J. Phys.: Condens. Matter* **2001**, *13* (40), 9001–9010.
(31) Hofmann, D. M.; Hofstaetter, A.; Leiter, F.; Zhou, H.; Henecker, F.; Meyer, B. K.; Orlinskii, S. B.; Schmidt, J.; Baranov, P. G. *Phys. Rev. Lett.* **2002**, *88* (4), 045504.
(32) Van de Walle, C. G. *Phys. Rev. Lett.* **2000**, *85* (5), 1012.
(33) Law, M.; Greene, L. E.; Johnson, J. C.; Saykally, R.; Yang, P. D. *Nat. Mater.* **2005**, *4* (6), 455–9.
(34) Keem, K.; Jeong, D. Y.; Kim, S.; Lee, M. S.; Yeo, I. S.; Chung, U. I.; Moon, J. T. *Nano Lett.* **2006**, *6* (7), 1454–1458.
(35) Pan, N.; Wang, X. P.; Zhang, K.; Hu, H. L.; Xu, B.; Li, F. Q.; Hou, J. G. *Nanotechnology* **2005**, *16* (8), 1069.
(36) Wu, J. J.; Wong, D. K. P. *Adv. Mater.* **2007**, *19* (15), 2015–2019.
(37) Ogawa, T.; Oikawa, H.; Kojima, A. *Jpn. J. Appl. Phys.* **1971**, *10* (5), 593.
(38) Agronin, A.; Molotskii, M.; Rosenwaks, Y.; Strassburg, E.; Boag, A.; Mutchnik, S.; Rosenman, G. *J. Appl. Phys.* **2005**, *97* (8), 84312.

(39) Morozovska, A. N.; Svechnikov, S. V.; Eliseev, E. A.; Jesse, S.; Rodriguez, B. J.; Kalinin, S. V. *J. Appl. Phys.* **2007**, *102* (11), 114108–14.
(40) Chubachi, N.; Iinuma, K.; Kikuchi, Y. *J. Appl. Phys.* **1971**, *42* (3), 962–7.
(41) Parsons, M. K.; English, F. L.; Hickerne, F. S. *J. Appl. Phys.* **1969**, *40* (6), 2369–71.
(42) Wilson, R. B. *J. Appl. Phys.* **1966**, *37* (4), 1932–1933.
(43) Blank, H.; Delavignette, P.; Gevers, R.; Amelinckx, S. *Phys. Status Solidi* **1964**, *7* (3), 747–764.
(44) Ogawa, T.; Kojima, A. *Appl. Phys. Lett.* **1966**, *8* (11), 294–296.
(45) Schulz, H.; Thiemann, K. H. *Solid State Commun.* **1979**, *32* (9), 783–5.
(46) Masetti, G.; Severi, M.; Solmi, S. *IEEE Trans. Electron Devices* **1983**, *ED/307*, 764–9.
(47) Casey, H. C., Jr.; Panish, M. B. *Heterostructure Lasers Part A*; Academic Press: New York, 1978.
(48) Hutson, A. R. *Phys. Rev.* **1957**, *108* (2), 222.
(49) Qu, Y.; Gessert, T. A.; Ramanathan, K.; Dhere, R. G.; Noufi, R.; Coutts, T. J. In *Electrical and optical properties of ion beam sputtered ZnO:Al films as a function of film thickness*; 39th National Symposium of the American Vacuum Society, Chicago, IL, 1993; AVS: Chicago, IL, 1993; pp 996−1000.
(50) Chen, M.; Pei, Z. L.; Wang, X.; Yu, Y. H.; Liu, X. H.; Sun, C.; Wen, L. S. *J. Phys. D: Appl. Phys.* **2000**, *33* (20), 2538–48.

NL080704N